# *Unsupervised seismic facies classification applied to a presalt carbonate reservoir, Santos Basin, offshore Brazil*

**Danilo Jotta Ariza Ferreira, Wagner Moreira Lupinacci, Igor de Andrade Neves, João Paulo Rodrigues Zambrini, André Luiz Ferrari, Luiz Antonio Pierantoni Gamboa, and Maria Olho Azul**

## ABSTRACT

Mapping of seismic and lithological facies is a very complex process, especially in regions with low seismic resolution caused by extensive salt layers, even when only an exploratory view of the distribution of the reservoir facies is required. The aim of this study was to apply multi-attribute analysis using an unsupervised classification algorithm to map the carbonate facies of an exploratory presalt area located in the Outer high region of the Santos Basin. The interval of interest is the Barra Velha Formation, deposited during the Aptian, which represents an intercalation of travertines, stromatolites, grainstones and spherulitic packstones, mudstones, and authigenic shales, which were deposited under hypersaline lacustrine conditions during the sag phase. A set of seismic attributes, calculated from a poststack seismic amplitude volume, was used to characterize geological and structural features of the study area. We applied k-means clustering in an approach for unsupervised seismic facies classification. Our results show that at least three seismic facies can be differentiated, representing associations of buildup lithologies, aggradational or progradational carbonate platforms, and debris facies. We quantitatively evaluated the seismic facies against petrophysical properties (porosity and permeability) from available well logs. Seismic patterns associated with the lithologies helped identify new exploration targets.

## INTRODUCTION

The Santos Basin is one of the largest sedimentary basins in Brazil, covering an area of approximately 350,000 km$^2$ (~135,000 mi$^2$).



Manuscript received March 1, 2018; provisional acceptance May 8, 2018; revised manuscript received June 11, 2018; final acceptance October 26, 2018.
DOI:10.1306/10261818055

## AUTHORS

Danilo Jotta Ariza Ferreira ~ *Department of Geology and Geophysics, Universidade Federal Fluminense, Brazil; daniloariza@id.uff.br*

Danilo Jotta Ariza Ferreira is geologist at Schlumberger and a Ph.D. candidate at Universidade Federal Fluminense (UFF). He received his B.S. degree (2015) from the State University of Rio de Janeiro and his M.S. degree (2018) from UFF. His research interests include carbonate reservoir characterization, sedimentology, and sequence stratigraphy.

Wagner Moreira Lupinacci ~ *Department of Geology and Geophysics, Universidade Federal Fluminense, Brazil; wagnerlupinacci@id.uff.br*

Wagner Moreira Lupinacci joined UFF in 2015 as a professor. He received his M.S. degree (2010) and his Ph.D. (2014) in reservoir and exploration engineering from State North Fluminense University. His technical expertise includes reservoir characterization and seismic inversion.

Igor de Andrade Neves ~ *Department of Geology and Geophysics, Universidade Federal Fluminense, Brazil; igor_neves@id.uff.br*

Igor de Andrade Neves graduated from Universidade Federal do Rio de Janeiro (UFRJ) in 2008 with a bachelor's degree in geology. In 2018, he completed his master's degree in geophysics working with a research project called Seismic Attribute Analysis and Inversion Applied for Presalt Reservoir Characterization. He is currently earning his Ph.D. in seismic interpretation at UFF.

João Paulo Rodrigues Zambrini ~ *Department of Geology and Geophysics, Universidade Federal Fluminense, Brazil; joaozambrini@gmail.com*

João Paulo Rodrigues Zambrini has a bachelor's degree in geophysics from the Universidade de São Paulo (USP) and a master's degree in petroleum reservoir engineering and exploration from the Universidade Estadual do Norte Fluminense in research on seismic processing data and Q filter analysis in porous media. Currently, he is a doctorate researcher at UFF working with presalt reservoir data.

André Luiz Ferrari ~ *Department of Geology and Geophysics, Universidade Federal Fluminense, Brazil; andreluizferrari@id.uff.br*

André Luiz Ferrari holds a degree in geology from UFRJ and a Ph.D. in geosciences from USP. He is an associate professor at UFF. He has experience in geosciences with an emphasis in structural geology, working mainly with rift basins, fractures and paleo tensions analysis, and tectonic sedimentation.

Luiz Antonio Pierantoni Gamboa ~ *Department of Geology and Geophysics, Universidade Federal Fluminense, Brazil; lgamboa@id.uff.br*

Luiz Antonio Pierantoni Gamboa graduated with a degree in geology in 1972 from UFRJ-Brazil, received a master's degree at Universidade Federal do Rio Grande do Sul in 1975, and earned a Ph.D. from Columbia University in 1981. He has taught at Texas A&M and joined Petrobras in 1985, working in the turbidites from the Campos Basin and with discoveries in the presalt section of Santos Basin. He joined UFF as a professor in 1987.

Maria Olho Azul ~ *Petrogal Brasil; mariaolhoazul@petrogalbrasil.com*

Maria Olho Azul is the lead development geologist at Petrogal Brasil. She received her M.S. degree (2012) from the University of Lisbon and has been working for the past 10 years with presalt carbonate reservoirs, focusing on reservoir modeling and characterization and implementation of rock typing workflows.

## ACKNOWLEDGMENTS

The authors thank Petrogal Brasil and the Brazilian National Agency of Petroleum, Natural Gas and Biofuels for providing field data and financial support for this research.

It is limited to the north by the Cabo Frio high, which separates it from the Campos Basin, and to the south by the Florianopolis high, which separates it from the Pelotas Basin. Three evolutionary phases of the basin are recognized (Moreira et al., 2007): the rift phase, the sag phase, and the drift phase.

The presalt reservoirs of the Santos Basin occur in both rift and sag phases, mainly in structural high regions. The main structural high of the basin is the Outer high (Gomes et al., 2002, 2008), which formed during a series of uplifts and erosions of rift shoulders during the Barremian. Distal positioning of this structural high led to low siliciclastic sedimentation that, in turn, induced presalt carbonate sedimentation in the region during the Aptian.

According to Szatmari and Milani (2016), the carbonate rocks of the Barra Velha Formation, upper sag phase, represent the largest nonmarine carbonate reservoirs in the world (reaching >500 m [>1640 ft] in thickness), which were deposited in shallow, highly alkaline lacustrine environments. Eruptions of basaltic lavas began in the rift phase and continued to occur such that they are intercalated with rocks of the sag phase, such as magnesium-rich authigenic shales, travertines, stromatolites, grainstones, and spherulitic packstones and mudstones. This recurrent volcanic and associated hydrothermal activity in the lacustrine environment of the sag phase together with erosion and leaching by superficial and subterranean water-mediated flow of, such as, Ca, Mg, and the compound $SiO_2$ from the surrounding volcanic terrain, provided the necessary conditions for the deposition of nonmarine carbonate facies. These lithologies eventually underwent subaerial exposure and wave reworking. In addition, through diagenetic $CO_2$ leaching of interdigitated volcanic rocks in the sequence, intense karstification of the reservoirs occurred, which increased porosity and permeability.

Wright (2012) reviewed several examples of lacustrine microbial carbonates, creating a facies distribution, architecture, composition, and diagenesis model for these environments. He suggests that these facies can be divided into four main types: (1) extensive carbonate platforms formed by microbial mats that have a plane-parallel architecture composed of bioherms or biostromes; (2) hydrothermal activity–controlled carbonate buildups at the edge of faults and isolated highs; (3) carbonate platform facies controlled by topography and bathymetry presenting aggradational or progradational architecture; and (4) mudstones and fine siliciclastic facies of lake bottoms. However, Wright and Barnett (2015) later proposed an abiotic model for the formation of these carbonates based on lake shallowing cycles; saturation of elements such as Ca, Mg, and $SiO_2$; and water Ph variation.

Della Porta (2015) also conducted a literature review on nonmarine carbonate sedimentation and pointed out that buildup facies and microbial mats are generally constituted of boundstones

or cementstones and that the detrital facies laterally associated with buildup eroded by waves or subaerial exposure are composed of pellets, spherulites, or intraclasts of stromatolites and travertines. The associated lithologies are packstones, grainstones, or floatstones.

The lacustrine carbonate facies of the sag phase in the Santos and Campos Basins have been associated with seismic facies in the regions of the Sapinhoá, Carcará, Itaipava, and Sagitário fields (Kattah and Balabekov, 2015) and in the Sugar Loaf high (Buckley et al., 2015). The seismic facies observed by these authors were generally classified as follows: (1) carbonate platforms of great areal extension, characterized by parallel to subparallel reflectors of moderate amplitude and with aggradational or progradational architecture; (2) isolated buildups nucleated above carbonate platforms and characterized by chaotic reflectors of moderate to low amplitude; (3) buildup alignments along main faulting zones; or (4) carbonate strings with evaporites around the bodies and reworking of facies by currents or subaerial exposure, characterized by chaotic to progradational reflectors with low to moderate amplitudes.

Saller et al. (2016) characterized the presalt rocks of the Kwanza Basin as seismic facies of carbonate platforms and fault-aligned buildups, comprising shrubby boundstones and spherulitic grainstones with intraclasts. These latter two facies types represent the best reservoir facies, which are intercalated with wackestones and packstones with intergranular dolomite. Microbial boundstones predominate in isolated buildup seismic facies, which are intercalated with wackestones, packstones, and grainstones composed of microbialite fragments. Seismic facies present in deeper regions of the sag phase are composed of stevensitic mudstones, with or without the presence of spherulites.

Seismic facies classification involves identifying patterns accounting for the variability among seismic attributes, thereby revealing information about geological features (Song et al., 2017). Generally, associated algorithms compare seismic attribute traces in an interval to generate clusters (Barnes and Laughlin, 2002). Importantly, the clusters reflect all the signals contained in the input data, that is, they can represent the continuity associated with geological and structural features, the redundancy related to strong correlations between attributes, and the noise created by artifacts that interfere with any classification process (Coléou et al., 2003).

Jesus et al. (2017) performed a very successful evaluation of a presalt reservoir area in the Santos Basin using hybrid spectral decomposition, maximum

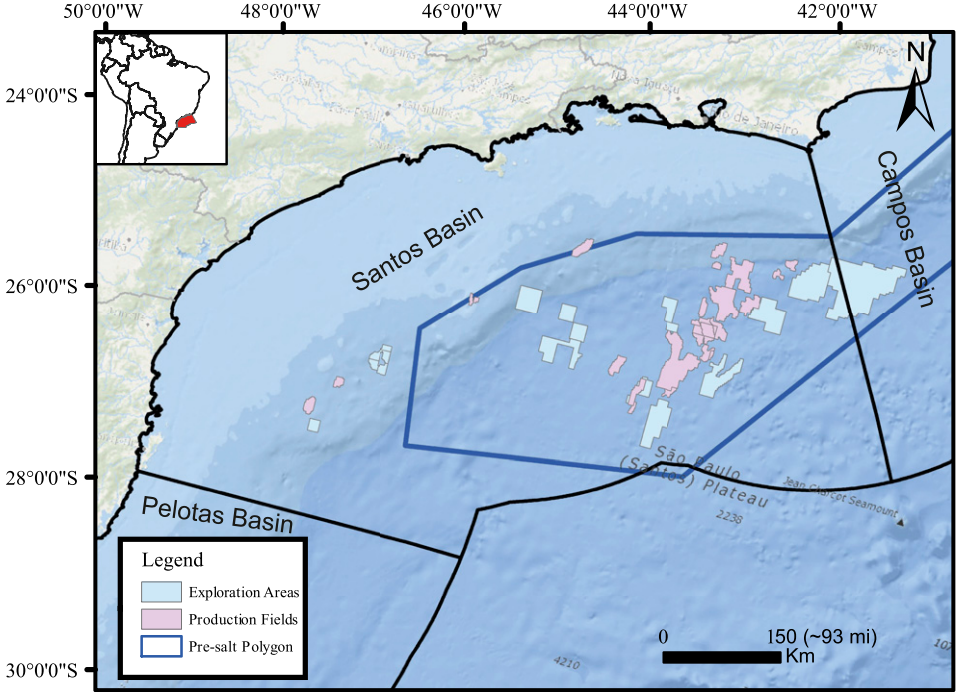


**Figure 1.** Location of the Santos Basin and its main production fields, exploration areas, and presalt main reservoirs of the Outer high.

curvature, and coherence attributes in an unsupervised classification by using a self-organizing maps approach, the objective of which was to individualize carbonate mounds, effectively demonstrating the feasibility of unsupervised classification methodologies for presalt areas.

Critical analyses of applied seismic attributes and reconstruction of the depositional model of a study area are essential to validate any classification process by unsupervised classification algorithms of a reservoir. Our objective was to identify geological and structural features and to perform a qualitative and quantitative characterization of the carbonate reservoirs of the Barra Velha Formation, focusing on an exploratory area located in the Outer high of the Santos Basin (Figure 1). To do this, we analyzed three seismic attributes and generated a multi-attribute seismic facies classification using k-means clustering.

## METHODOLOGY

Our data set consisted of a poststack seismic volume and well logs from four wells provided by the company Galp Energia. A prestack depth migration flow was performed, focused on imaging of presalt layers, and basically consisted of initial velocity model building, three sediment tomography stages (salt flood, intra salt, and presalt), final Kirchhoff migration, residual multiple reduction, stacking, and poststack processing. The region of the seismic survey, well locations, and inlines or arbitrary lines represented in this study are shown in Figure 2. Principal component analysis (PCA) was employed to aid in the determination of attributes to be used, and multi-attribute classification of the seismic facies was performed using a k-means clustering algorithm (both detailed below).

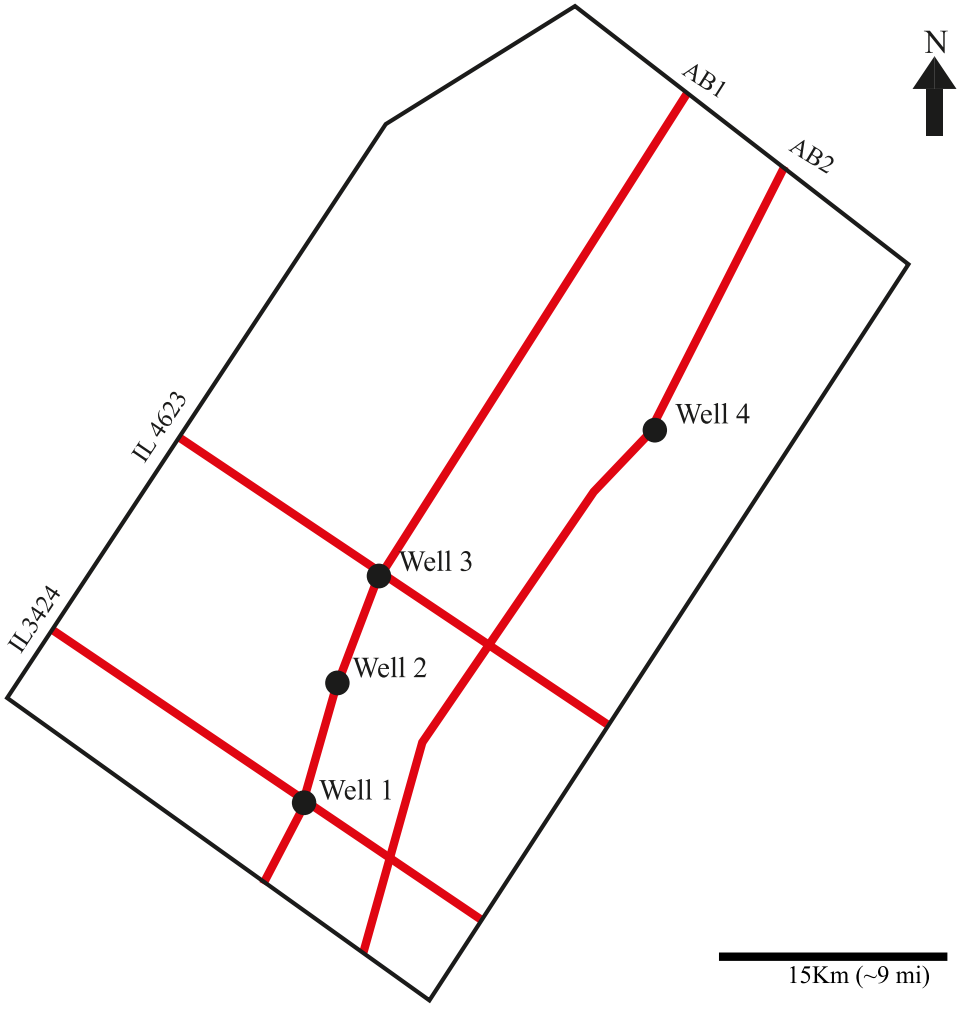


**Figure 2.** Region of the seismic survey, well locations, and inlines (IL) or arbitrary lines (AB) represented in this study.

Depositional characteristics of lacustrine carbonate environments and, more specifically, analogs of the Santos, Campos, and Kwanza Basin sag phases were used to create a conceptual model of the reservoirs to assist in our seismic facies characterization of the Barra Velha Formation. A preconditioning workflow was applied before the seismic inversion to improve resolution and to increase the signal-to-noise ratio. This workflow consisted of applying filters to remove noise and to recover the attenuation effects (described in Lupinacci et al., 2017).

Seismic interpretations of the top and bottom of the Barra Velha Formation, represented respectively by the upper Aptian (base of salt layer) and lower Aptian (Sub-Alagoas) surfaces, were performed according to seismic reflection termination patterns that indicate sequence limits and surfaces delimiting seismic units and depositional system tracts, with the most commonly used being onlap, downlap, toplap, lapout, truncation, and conformity. Seismic reflections preserve the geological factors that generated them, such as stratification, lithology, and depositional features (Brown and Fisher, 1977). The interpreted seismic-stratigraphic horizons in an inline are shown in Figure 3.

We then studied the seismic patterns using amplitude seismic data and several seismic attributes calculated from amplitude, phase, and frequency for our unsupervised facies classification. Finally, we selected three attributes that best represented geological meaning to be employed: two stratigraphic attributes (acoustic impedance and envelope) and one structural attribute (high-resolution eigenstructure-based coherence). Acoustic impedance was derived using the model-based method defined by Russell and Hampson (1991), the envelope was calculated from the method proposed by Taner et al. (1979), and our estimate of the high-resolution eigenstructure-based coherence followed the method proposed by Gersztenkorn and Marfurt (1999). This analysis identified three seismic patterns of the lacustrine carbonate depositional subenvironments: buildups, debris facies, and aggradational or progradational carbonate platforms. Type representations of those seismic patterns and their features are provided in Figure 4.

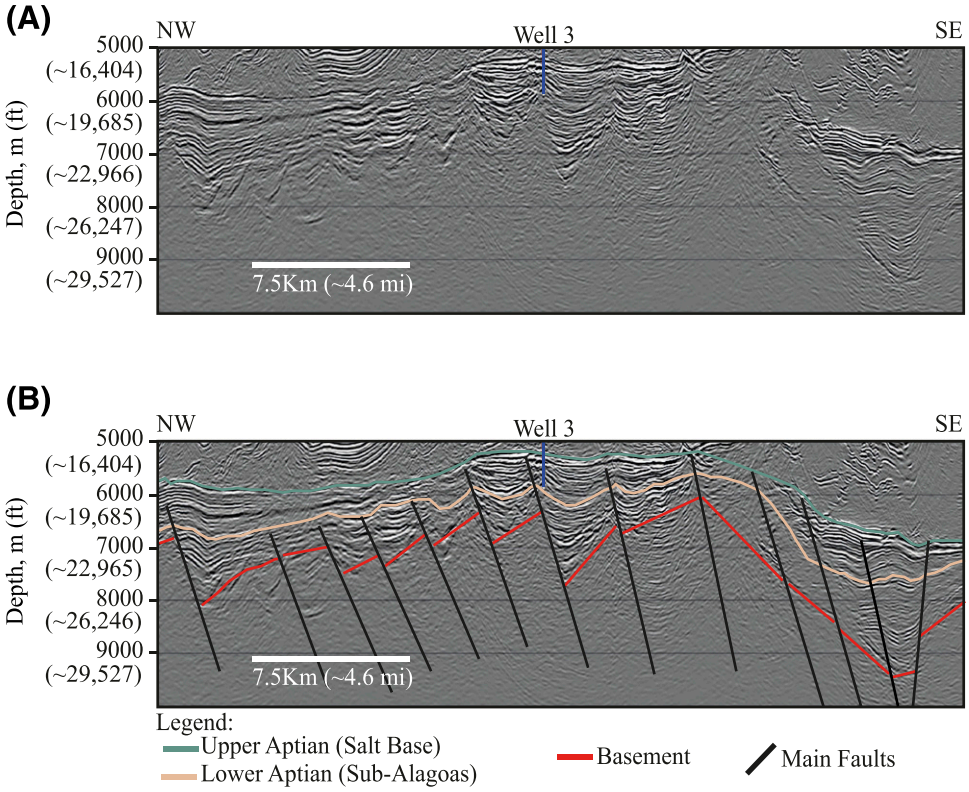


**Figure 3.** (A) Uninterpreted seismic section and (B) interpreted seismic section with presalt seismic–stratigraphic surfaces and main faults for the region of interest.

| Seismic Attributes | Seismic Patterns | | | Scale |
|---|---|---|---|---|
| | Build-up | Debris | Aggradational or Progradational Carbonate Platforms | |
| Amplitude | 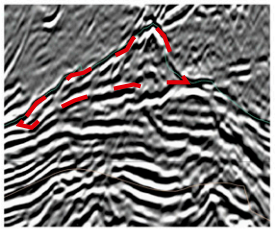 | 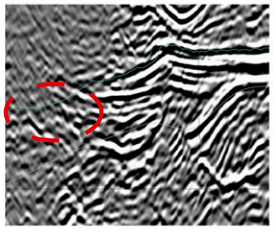 | 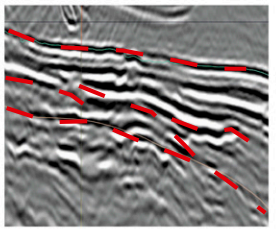 |   |
| Acoustic Impedance | 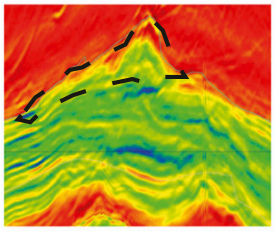 | 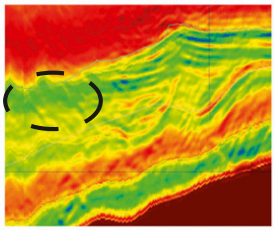 | 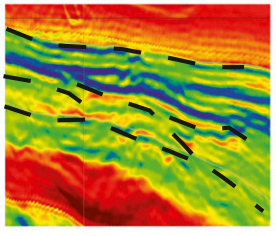 |   |
| Envelope | 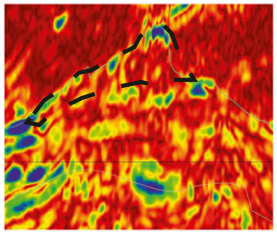 | 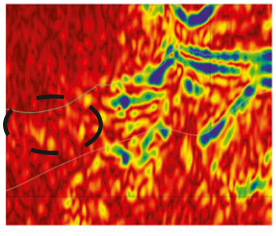 | 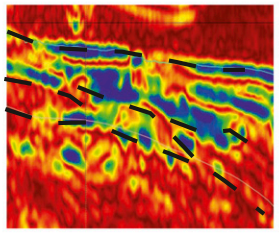 |   |
| High-resolution Eigen | 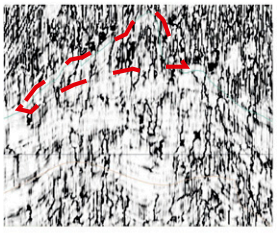 | 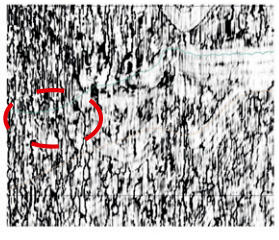 | 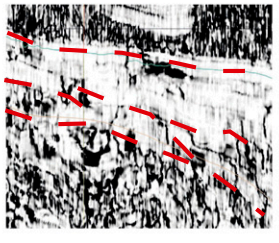 |   |
| Seismic Signal | Amplitude: well marked conical geometry with chaotic internal reflectors;<br>Acoustic Impedance: low to medium values varying from the base to the top;<br>Envelope: marked conical geometry;<br>Eigen: lots of internal fractures. | Amplitude: chaotic internal reflectors;<br>Acoustic Impedance: medium values;<br>Envelope: absent to low signal;<br>Eigen: chaotic internal pattern. | Amplitude: when aggradational presents plane-parallel reflectors, when progradational presents lobate shape reflectors;<br>Acoustic Impedance: when aggradational presents intercalated medium to high values, when progradational, presents intercalated low to medium values;<br>Envelope: when aggradational, presents well-marked internal and external geometry, when progradational, presents marked external geometry;<br>Eigen: when aggradational, presents almost absent fracturing, when progadational presents internal fracturing. | |

**Figure 4.** Type representations of main seismic patterns and their features for the original seismic and selected attributes. The red and black dashed lines indicate the seismic patterns in the given examples.

Following the observation of the seismic patterns in the selected attributes, we performed an unsupervised seismic facies classification using k-means clustering method in conjunction with PCA. Zhao et al. (2015) defined PCA as a data projection technique that aims to reduce the size of the sample space to be classified by identifying the main components (or higher variance directions), called eigenvectors, thereby reducing redundancy and noise of the sample space. Definition of the eigenvectors consisted of a cross-correlation analysis among all input volumes and identification of the vector with the greatest variance. This vector was then rescaled and subtracted from the original sample space before a second main component vector was calculated from within the residual sample space. This process was repeated until all vectors representing the data set had been established. Then, user-defined eigenvectors, the ones that represent the most percentage of the sample space, were used in the classification algorithm.

The first stage of the k-means clustering algorithm (Macqueen, 1967; Zhao et al., 2015) begins with choosing the number of facies or clusters into which the sample space will be divided. The seed points of each cluster are randomly positioned in the sample space, and the Euclidean distances between the seeds and the data points in the sample space are calculated. Then, the data points in the sample space are associated with the cluster represented by the nearest seed point. Finally, the seed points are centered in relation to the cluster of data points that they represent, and new iterations of this process are performed until the association of each data point in the sample space with a given cluster is well defined.

**Table 1.** Cross-Correlation Matrix between the Attribute Eigenvectors Used in Our Unsupervised Multi-Attribute Seismic Facies Classification

| Cross-Correlation Matrix | Acoustic Impedance, % | High-Resolution Eigen, % | Envelope, % |
|---|---|---|---|
| Acoustic impedance | 100 | 2 | 8 |
| High-resolution eigen | 2 | 100 | 20 |
| Envelope | 8 | 20 | 100 |

**Table 2.** Representativeness of Each of the Principal Component Analysis Eigenvectors Generated in Relation to the Total Sample Space

| PCA Volume Representativity | Individual, % | Cumulated, % |
|---|---|---|
| PCA1 | 41 | 41 |
| PCA2 | 33 | 74 |
| PCA3 | 26 | 100 |

Abbreviation: PCA = principal component analysis.

For our study, the input volumes in the unsupervised classification algorithm were the volumes resulting from the analysis of principal components performed with the three volumes of selected attributes: acoustic impedance, envelope, and high-resolution eigenstructure-based coherence.

Table 1 shows that there is little redundancy among the seismic attributes, given the low values of the cross-correlation matrix. The cross-correlation matrix in Table 2 shows that the sample space is largely represented by each of the individual PCA

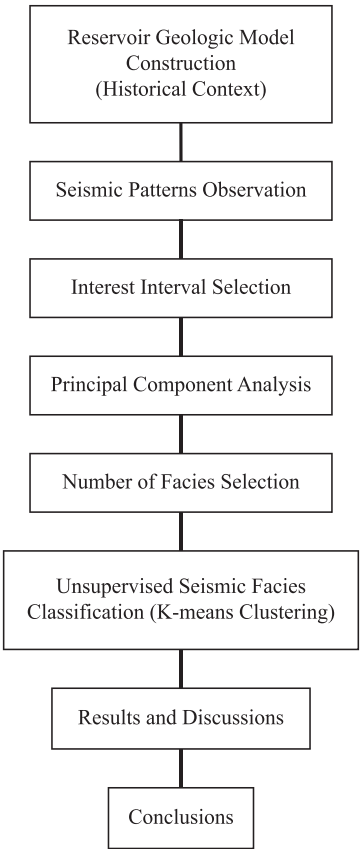


**Figure 5.** Proposed workflow used in this work for the unsupervised seismic facies classification.

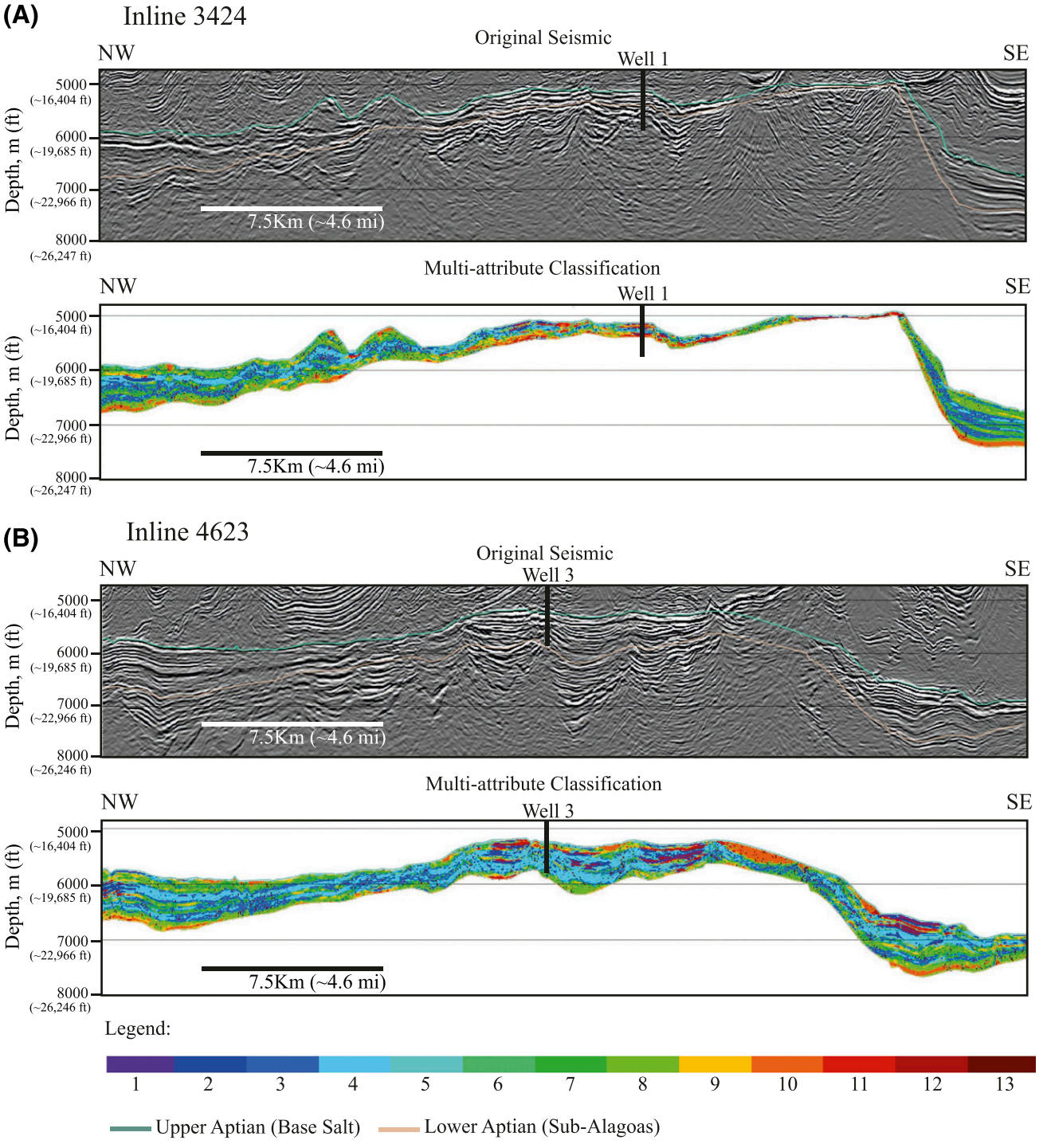


**Figure 6.** Comparisons between seismic patterns in the original volume and the results of our multi-attribute seismic facies classification for (A) inline 3424 that intersects Well 1 and (B) inline 4623 that intersects Well 3.

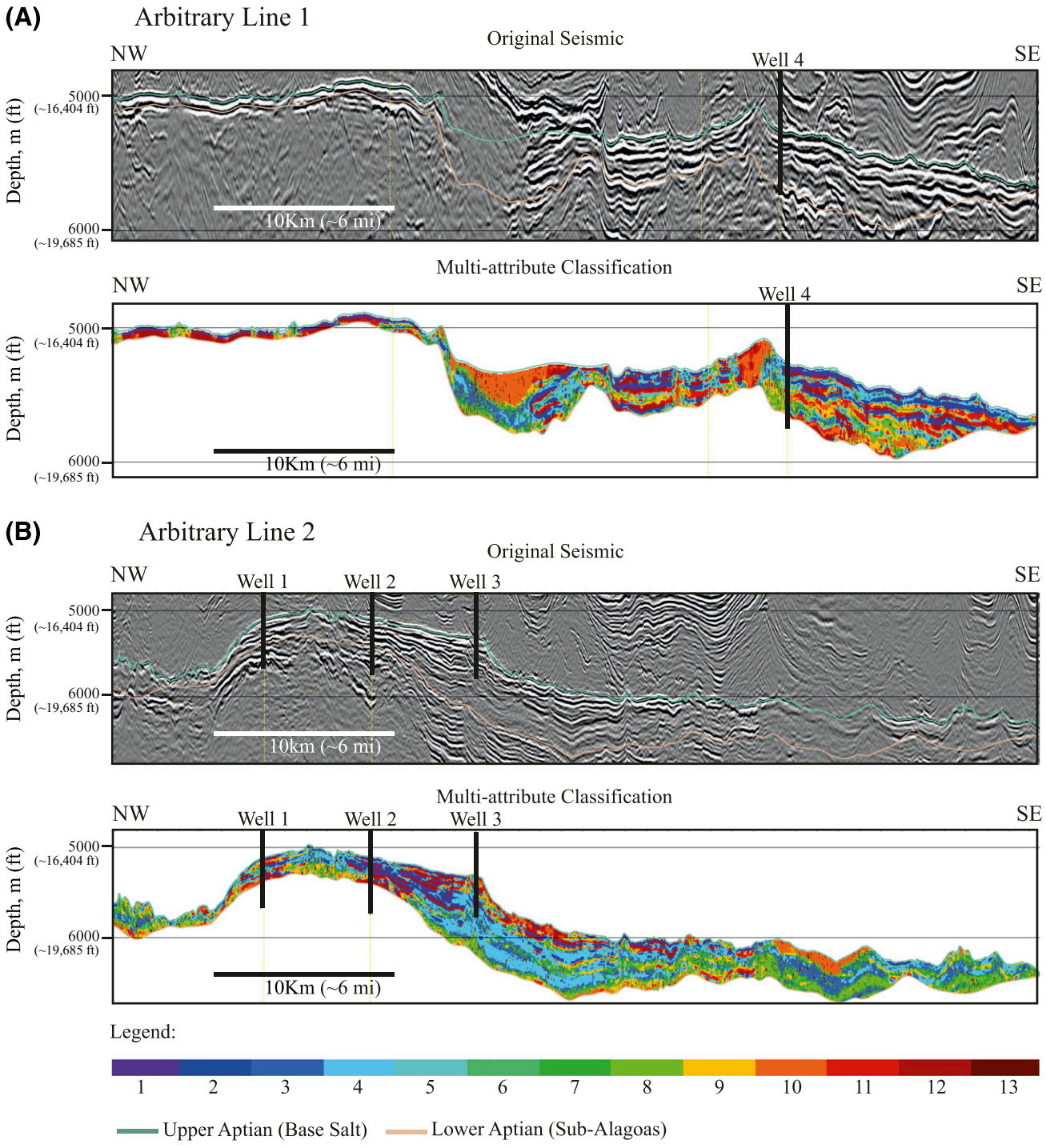


**Figure 7.** Comparisons between seismic patterns in the original volume and the results of our multi-attribute seismic facies classification for (A) arbitrary line (AB)1 that intersects Well 4 and (B) AB2 that intersects Wells 1, 2, and 3.

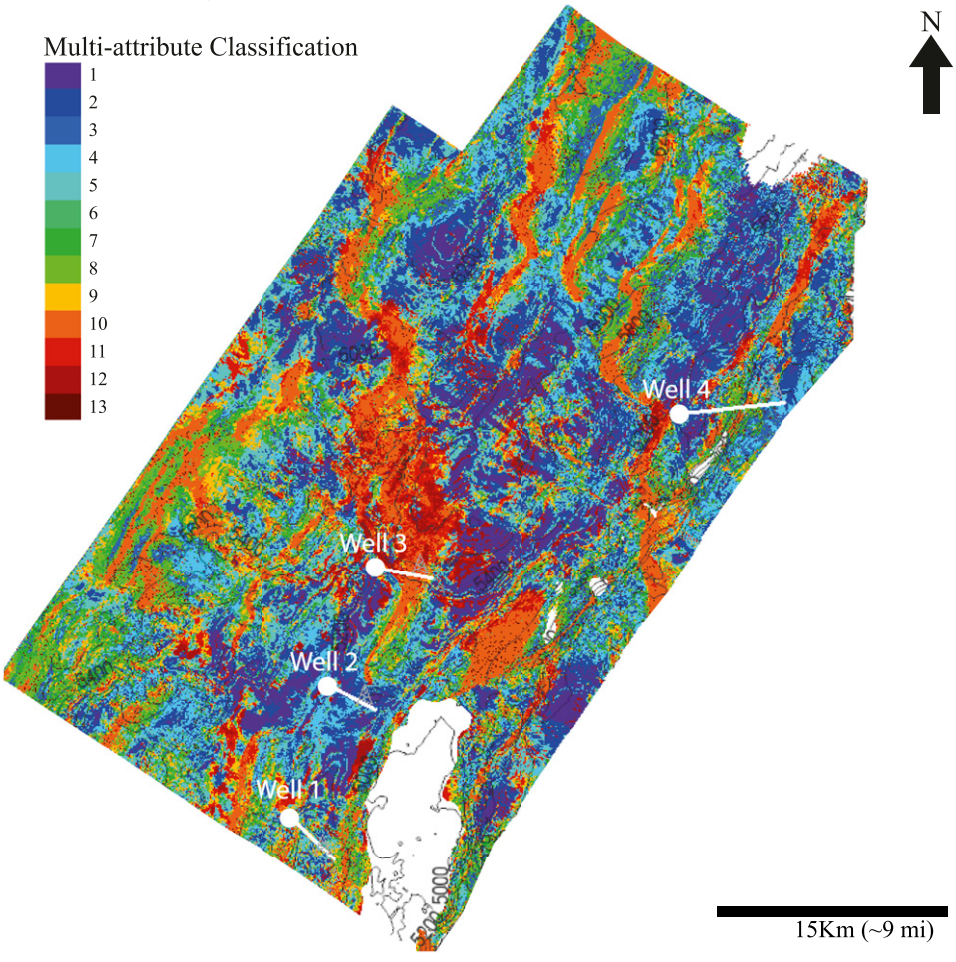


**Figure 8.** Multi-attribute classification of seismic facies for the surface of the upper Aptian that represents the top of the main reservoirs of the Barra Velha Formation.

volumes used in our k-means classification algorithm. Although the number of PCA eigenvectors is equal to the number of seismic attributes we used, they can still better represent with greater geological coherence the original sample space, further reducing the low redundancy between attributes and limiting the influence of noise in the data set.

We performed our multi-attribute seismic facies classification with k-means clustering using 13 seeds, with this number being based on a trial-and-error approach in which several cluster numbers were attempted between 3 to 20 clusters. Each result was visually evaluated and compared with the seismic patterns recognized in the amplitude seismic data to choose the cluster number that best related to geological and structural features. The workflow we used is summarized in Figure 5.

## RESULTS AND DISCUSSION

A comparison of the seismic patterns and the results of our unsupervised multi-attribute seismic facies classification for inlines (northwest–southeast) perpendicular to the main directions of syn-rift faults of the Santos Basin are shown in Figure 6. In Figure 7 we show this comparison for arbitrary lines (southwest–northeast) parallel to the largest syn-rift faults. In addition, in Figure 8 we show the results of our multi-attribute seismic facies classification for the surface of the upper Aptian. These three figures show that seismic facies 1, 2, 3, 4, 11, and 12 predominate in the flat or soft ramp regions of structural highs, whereas the seismic facies 5, 6, 7, 8, 9, and 10 predominate on the edges of these highs or in local highs. Seismic facies 1, 2, 3, 4, 10, 11, and 12 also occur in structural lows.

Wells 1 and 2 were drilled in areas of aggradational or progradational platforms, where the results

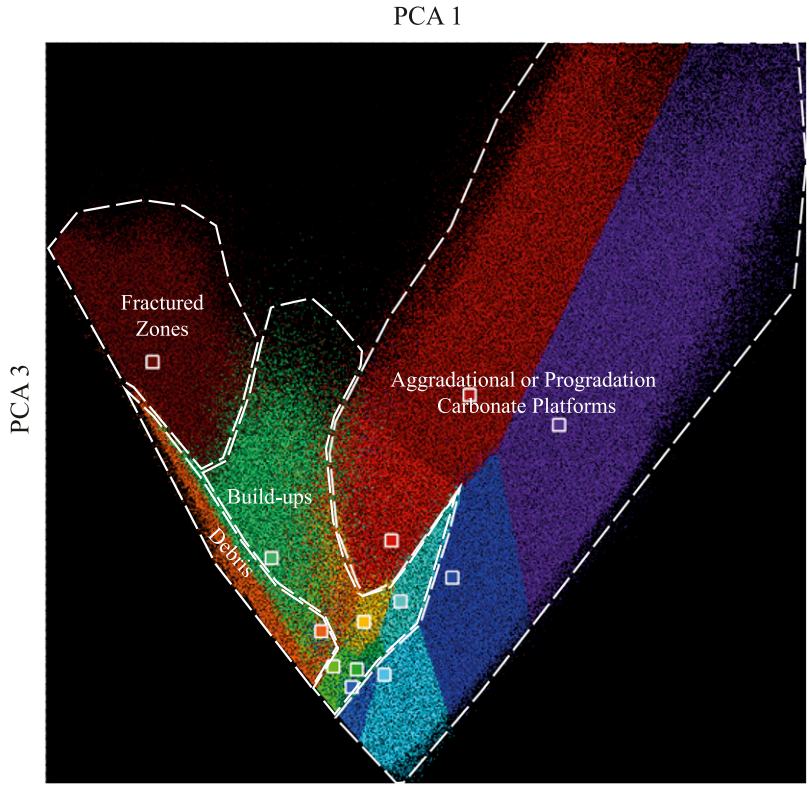


**Figure 9.** Crossplot between the principal component analysis (PCA) eigenvectors revealing individual representability in the sample space. The white polygons associate the multi-attribute seismic facies classification with the observed seismic patterns.

of our multi-attribute seismic classification point to intercalation of seismic facies 1, 2, 3, 4, 11, and 12. Well 3 was drilled in a region with a preponderance of buildups in the basal and intermediate parts and debris facies at the top. The results of our seismic classification for the area of this well indicate that intercalation of seismic facies 5, 6, 7, 8, and 9 occur in the basal and intermediate parts and that seismic facies 10 predominates as the top. Well 4 was drilled in an area consisting largely of buildups at the base and aggradational or progradational platforms at the top. Our multi-attribute seismic facies classification reveals a predominance of seismic facies 5, 6, 7, 8, and 9 at the basal part of this area and seismic facies 1, 2, 3, 4, 11, and 12 at the top.

Figure 9 shows a crossplot for the PCA eigenvectors, revealing individual representability in the sample space. The white polygons link the multi-attribute seismic facies with observed seismic patterns. As can be noted, the clusters discriminate seismic patterns very well, even if little overlapping exists. Seismic facies 1, 2, 3, 4, 11, and 12 are associated with intercalations of carbonate platforms. Seismic facies 5, 6, 7, 8, and 9 represent buildups. Seismic facies 10 reflects debris facies, and seismic facies 13 is associated with fracture zones.

We present correlations of our multi-attribute seismic facies classification with well log analysis

**Table 3.** Comparison of the Porosity and Permeability Well Log Results (Based on Total Magnetic Resonance–Derived Porosity and Neutron Logs) with the Recognized Seismic Patterns

| Seismic Patterns | Mean Porosity, % | Mean Permeability, md |
|---|---|---|
| Aggradational or progradational carbonate platform (low-impedance layers) | 11.5 | 17 |
| Aggradational or progradational carbonate platform (high-impedance layers) | 7 | 6.7 |
| Buildups | 9 | 17 |
| Debris | 11 | 21.3 |
| Fractured zones | 10 | 5.3 |

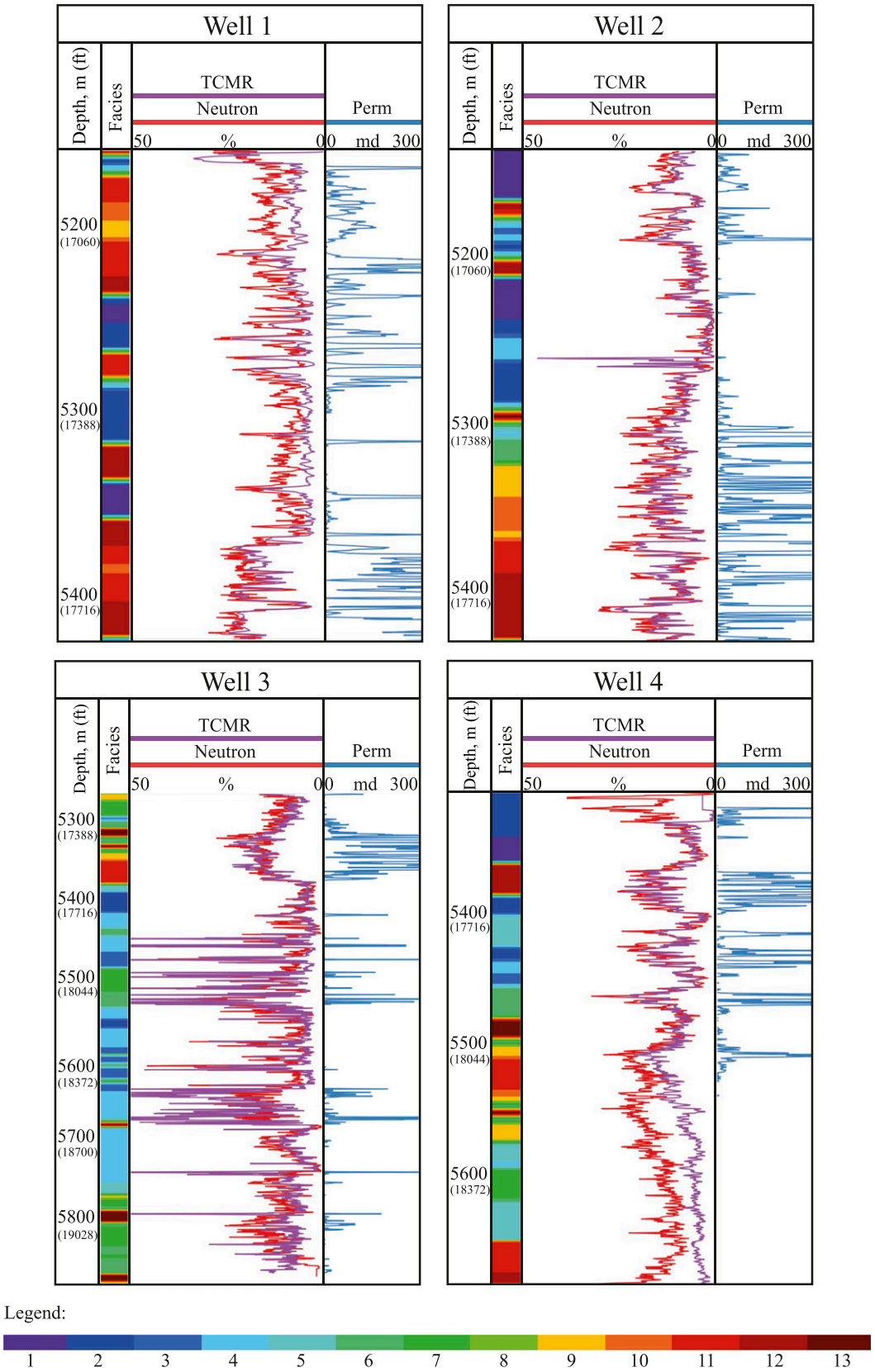


**Figure 10.** Comparison of multi-attribute seismic facies classification (Facies) results with porosity and permeability (Perm) data derived from total magnetic resonance–derived porosity (TCMR) and neutron well log data, in meters (feet in parentheses).

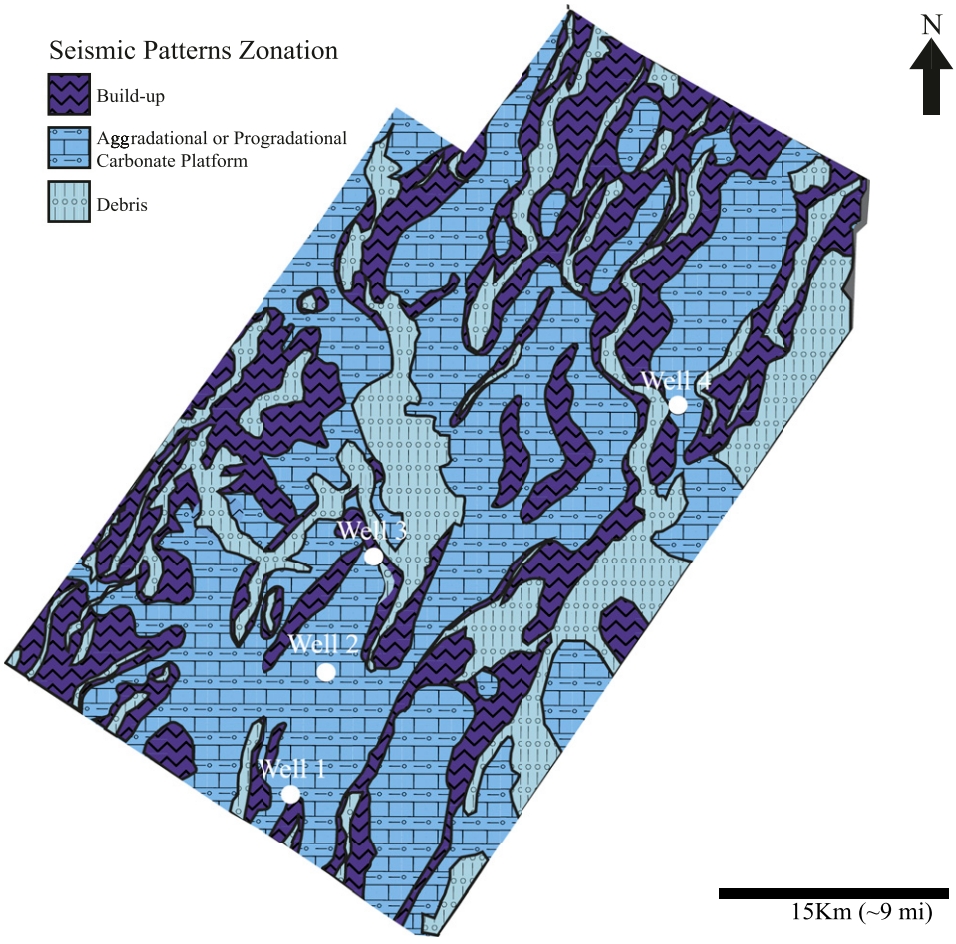


**Figure 11.** Seismic pattern area zonation at the upper Aptian surface.

in Table 3 and Figure 10. This comparison of the seismic facies with porosity and permeability was done by analyzing mean porosity and permeability values, obtained from the magnetic resonance (total magnetic resonance–derived porosity) and neutron well logs, with the multi-attribute seismic facies present in the well locations. These results show that seismic facies 5, 6, 7, 8, and 9 (i.e., associated with buildups) collectively exhibit a mean porosity of 9% and a mean permeability of 17 md. Seismic facies associated with debris patterns present mean porosity and mean permeability values of 11% and 21.3 md, respectively.

Aggradational or progradational carbonate platforms exhibit two sets of seismic facies, one with the lowest values of porosity and permeability (7% and 6.7 md, respectively, represented by seismic facies 1, 2, 3, and 4) and another set with the highest porosity and permeability values (11.5% and 17 md, respectively, represented by seismic facies 11 and 12).

Conceptual geological models for the study area generated through the zonation of seismic patterns related to their multi-attribute seismic facies, as established in Figure 9, for the upper Aptian surface and inline 3424 are shown in Figures 11 and 12, respectively. These models support the idea proposed by several previous studies (Wright, 2012; Della Porta, 2015; Saller et al., 2016) that the seismic patterns of buildups predominantly lie at the edges of the southwest–northeast faults but also can be observed at local highs as isolated buildups, possibly with stromatolites or shrubs as associated lithologies.

The aggradational or progradational carbonate platforms' seismic patterns are found in flat or soft-ramp regions of both structural highs and structural lows. These carbonate platforms in the structural lows may be connected to muddier carbonate lithologies, whereas in the structural highs, they are connected to the carbonate sedimentation originating from microbiological mats or spherulitic precipitation.

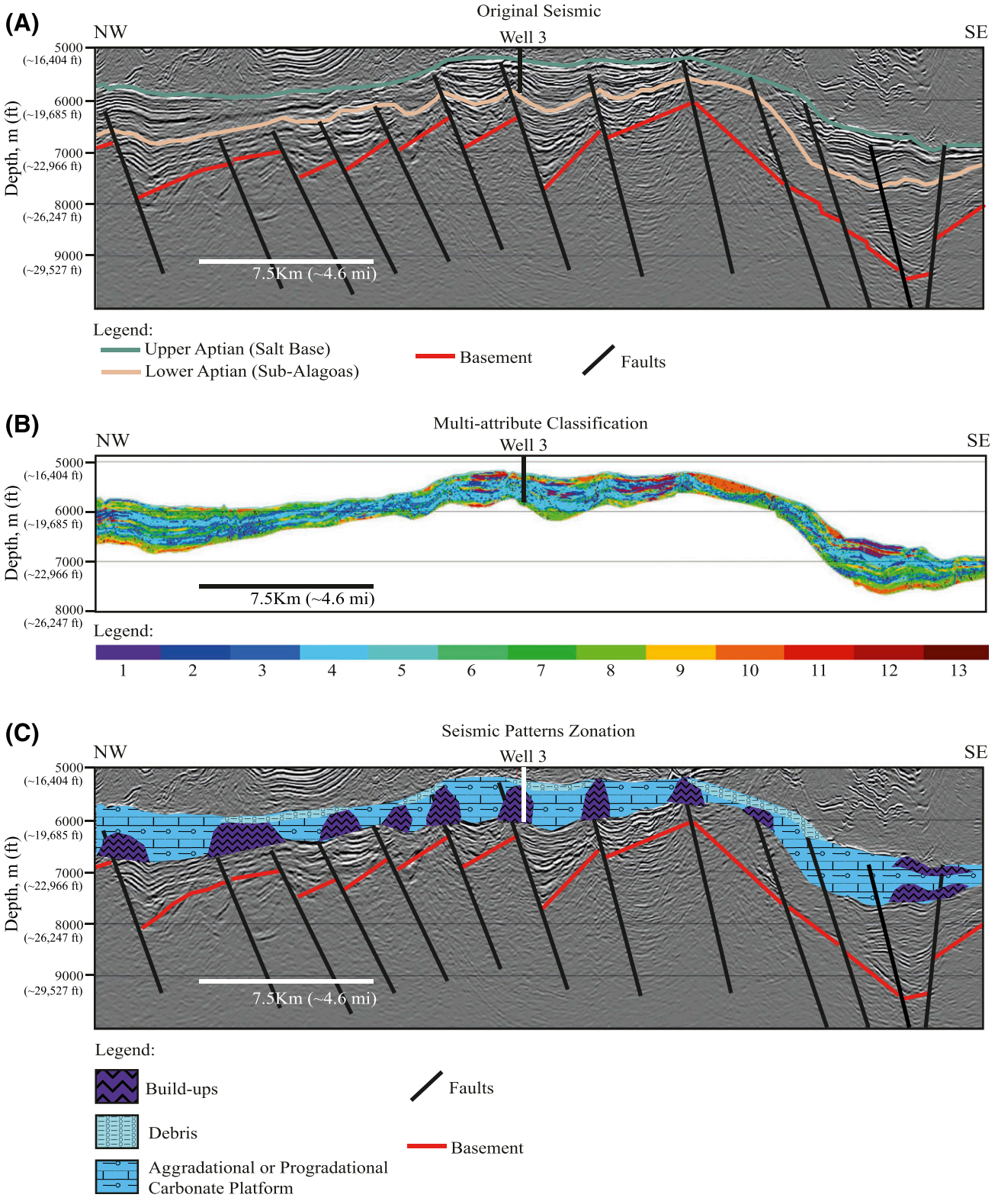


**Figure 12.** Seismic pattern area zonation for inline 3424, showing (A) the original seismic pattern, (B) the multi-attribute seismic facies classification results, and (C) seismic pattern zonation.

Finally, the debris seismic patterns are always in the lower terrain near the edges of faults and are possibly related to wave or subaerial reworking of facies during periods of lower lacustrine water levels. The lithologies associated with debris seismic patterns are probably grainstones, packstones, and wackestones with stromatolitic and spherulitic intraclasts.

## CONCLUSIONS

We generated an unsupervised multi-attribute seismic facies classification using a k-means clustering approach based on seismic attributes to identify seismic patterns and to facilitate qualitative and quantitative characterization of the sag-phase reservoirs in the study area. We could identify and characterize three seismic patterns based on their seismic facies: buildups, aggradational or progradational carbonate platforms, and debris facies. By comparing our multi-attribute seismic facies classification and well log data, we could establish that the most porous and permeable multi-attribute seismic facies are those associated with patterns of buildups, low-impedance aggradational or progradational carbonate platform layers, and debris facies. The results of our multi-attribute seismic facies classification allowed us to build a map of the top level of the reservoirs and a section view of the sag phase reflecting seismic pattern associations in the region to predict the best prospective drilling areas.

## REFERENCES CITED


Barnes, A. E., and K. J. Laughlin, 2002, Investigation of methods for unsupervised classification of seismic data, *in* Society of Exploration Geophysicists Technical Program Expanded Abstracts 2002, Salt Lake City, Utah, October 6–11, 2002, p. 2221–2224, doi:10.1190/1.1817152.

Brown, L. F. Jr., and W. L. Fisher, 1977, Seismic stratigraphy interpretation of depositional surfaces: Examples from Brazilian rift and pull-apart basins, *in* C. E. Payton, ed., Seismic stratigraphy: Applications to hydrocarbon exploration: AAPG Memoir 26, p. 213–248.

Buckley, J. P., D. Bosence, and C. Elders, 2015, Tectonic setting and stratigraphic architecture of an Early Cretaceous lacustrine carbonate platform, Sugar Loaf High, Santos Basin, Brazil: Geological Society, London, Special Publications 2015, v. 418, p. 175–191, doi:10.1144/SP418.13.

Coléou, T., M. Poupon, and K. Azbel, 2003, Unsupervised seismic facies classification: A review and comparison of techniques and implementation: Leading Edge, v. 22, no. 10, p. 942–953, doi:10.1190/1.1623635.

Della Porta, G., 2015, Carbonate build-ups in lacustrine, hydrothermal and fluvial settings: Comparing depositional geometry, fabric types and geochemical signature, *in* D. W. J. Bosence, K. A. Gibbons, D. P. Le Heron, W. A. Morgan, T. Pritchard, and B. A. Vining, eds., Microbial carbonates in space and time: Implications for global exploration and production: Geological Society, London, Special Publications 2015, v. 418, p. 17–68, doi:10.1144/SP418.4.

Gersztenkorn, A., and K. J. Marfurt, 1999, Eigenstructure-based coherence computations as an aid to 3-D structural and stratigraphic mapping: Geophysics, v. 64, no. 5, p. 1468–1479, doi:10.1190/1.1444651.

Gomes, P. O., B. Kilsdonk, J. Minken, T. Grow, and R. Barragan, 2008, The outer high of the Santos Basin, Southern São Paulo Plateau, Brazil: Pre-salt exploration outbreak, paleogeographic setting, and evolution of the syn-rift structures: AAPG International Conference and Exhibition, Cape Town, South Africa, October 26–29, 2008, p. 26–29.

Gomes, P. O., J. Parry, and W. Martins 2002, The outer high of the Santos Basin, Southern São Paulo plateau, Brazil: Tectonic setting, relation to volcanic events and some comments on hydrocarbon potential: AAPG Search and Discovery article 10193, accessed December 22, 2017, http://www.searchanddiscovery.com/pdfz/documents/2009/10193gomes/images/gomes.pdf.html.

Jesus, C., M. O. Azul, W. Lupinacci, and L. Machado, 2017, Mapping of carbonate mounds in the Brazilian presalt zone, *in* Society of Exploration Geophysicists Technical Program Expanded Abstracts 2017, Houston, Texas, September 24–29, 2017, p. 3298–3303, doi:10.1190/segam2017-17789870.1.

Kattah, S., and Y. Balabekov, 2015, Seismic facies/geometries of the pre-salt limestone units and newly-identified exploration trends within the Santos and Campos basins, Brazil: 14th International Congress of the Brazilian Geophysical Society and EXPOGEF, Rio de Janeiro, Brazil, August 3–6, 2015, p. 288–293, doi:10.1190/sbgf2015-057.

Lupinacci, W. M., A. Peixoto de Franco, S. A. M. Oliveira, and F. Sergio de Moraes, 2017, A combined time-frequency filtering strategy for Q-factor compensation of poststack seismic data: Geophysics, v. 82, no. 1, p. V1–V6, doi:10.1190/geo2015-0470.1.

MacQueen, J., 1967, Some methods for classification and analysis of multivariate observations, *in* Proceedings of the 5th Berkeley Symposium on Mathematical Statistics and Probability, Volume 1: Statistics: Oakland, California, University of California Press, p. 281–297.

Moreira, J. L. P., C. V. Madeira, J. A. Gil, and M. A. P. Pinheiro, 2007, Bacia de Santos: Boletim de Geociencias da Petrobras, v. 15, no. 2, p. 531–549.

Russell, B., and D. Hampson, 1991, Comparison of poststack seismic inversion methods, *in* Society of Exploration Geophysicists Technical Program Expanded Abstracts 1991,

Houston, Texas, November 10–14, 1991, p. 876–878, doi:10.1190/1.1888870.
Saller, A., S. Rushton, L. Buambua, K. Inman, R. McNeil, and J. A. D. T. Dickson, 2016, Presalt stratigraphy and depositional systems in the Kwanza Basin, offshore Angola: AAPG Bulletin, v. 100, no. 7, p. 1135–1164, doi:10.1306/02111615216.
Song, C., Z. Liu, H. Cai, Y. Wang, X. Li, and G. Hu, 2017, Unsupervised seismic facies analysis with spatial constraints using regularized fuzzy c-means: Journal of Geophysics and Engineering, v. 14, no. 6, p. 1535–1543, doi:10.1088/1742-2140/aa8433.
Szatmari, P., and E. J. Milani, 2016, Tectonic control of the oil-rich large igneous-carbonate-salt province of the South Atlantic rift: Marine and Petroleum Geology, v. 77, p. 567–596, doi:10.1016/j.marpetgeo.2016.06.004.
Taner, M. T., F. Koehler, and R. E. Sheriff, 1979, Complex seismic trace analysis: Geophysics, v. 44, no. 6, p. 1041–1063, doi:10.1190/1.1440994.
Wright, V. P., 2012, Lacustrine carbonates in rift settings: The interaction of volcanic and microbial processes on carbonate deposition: Geological Society, London, Special Publications 2012, v. 370, p. 39–47, doi:10.1144/SP370.2.
Wright, V. P., and A. J. Barnett, 2015, An abiotic model for the development of textures in some South Atlantic early Cretaceous lacustrine carbonates: Geological Society, London, Special Publications 2015, v. 418, p. 209–219, doi:10.1144/SP418.3.
Zhao, T., V. Jayaram, A. Roy, and K. J. Marfurt, 2015, A comparison of classification techniques for seismic facies recognition: Interpretation, v. 3, no. 4, p. SAE29–SAE58, doi:10.1190/INT-2015-0044.1.